



Climate Modes evaluation datasets from CMIP6 pre-industrial control simulations and observations

Sandeep Mohapatra^{1,2}, Alex Sen Gupta^{1,3}, Nathaniel L. Bindoff^{1,2,4}, Yuxuan Lyu^{1,2}

- Australian Centre for Excellence in Antarctic Science, University of Tasmania, Hobart, Australia
 - ²Institute for Marine and Antarctic Studies, University of Tasmania, Hobart, Australia
 - ³Climate Change Research Centre, University of New South Wales, Sydney, Australia
 - ⁴ Australian Antarctic Program Partnership, University of Tasmania, Hobart, Australia

Correspondence to: Sandeep Mohapatra (sandeep.mohapatra@utas.edu.au)

10

15

20

25

30

5

Abstract

Internal climate variability encompasses processes ranging from daily weather fluctuations to multidecadal interactions within the climate system. A large component of internal variability on sub-seasonal to multi-decadal time scales is associated with recurring patterns or "climate modes". In this study we provide an openly available dataset of eight major climate modes: Eastern Pacific El Niño (EP-El Niño), Central Pacific El Niño (CP-El Niño), Interdecadal Pacific Oscillation (IPO), Indian Ocean Dipole (IOD), Subsurface Dipole Mode (SDM), Atlantic Multidecadal Oscillation (AMO), North Atlantic Oscillation (NAO), and Southern Annular Mode (SAM). These modes were derived from 23 Coupled Model Intercomparison Project 6 (CMIP6) models, each with over 500 years of simulation data, ensuring robust statistical insights into their spatial and temporal structures. The datasets were validated against observational data, revealing broad-scale consistency and highlighting biases in regional features and amplitudes. However, regional discrepancies, like exaggerated warming or cooling in specific areas, were found. Despite these limitations, the datasets provide an important resource for understanding climate variability, conducting detection and attribution studies, and improving climate projections. All datasets are publicly accessible (Mohapatra et al. 2025; https://doi.org/10.5281/zenodo.17337105), supporting future research and policy development to address climate variability and its implications for climate change adaptation and mitigation.

Short Summary



40

45

50

55

60

65



This study provides a new open-access datasets that capture how natural climate patterns shape the global climate. The datasets are built from climate model simulations and observations, allowing researcher to see how well models reproduce natural climate behaviour. Our openly available datasets will help researchers to better distinguish natural climate variability from human-caused changes. These resources also provide a foundation for improving climate models and long-term projections.

1 Introduction

1.1 Internal variability and Climate Modes

Identifying internal variability is crucial for isolating the anthropogenic climate change signal, which can enhance or mask the long-term trend (Deser et al., 2012; Kay et al., 2015). A better understanding of internal processes is an important factor in reducing the uncertainty of climate projections. The internal variability of the climate system can be described, to a large extent, as a combination of climate modes. A climate mode is a recurring pattern of climate variability that typically spans large geographical areas and influences weather and climate over weeks to decades. These patterns emerge from complex interactions between the atmosphere, oceans, and sometimes land or ice systems. Each mode is usually characterized by specific spatial patterns (such as sea surface temperature or sea level pressure anomalies) and temporal behaviour (how often it occurs and how long it lasts).

1.2 Climate Modes across the Globe

Different ocean basins host various climate modes operating at multiple time scales, ranging from sub-seasonal to interannual, decadal, and multidecadal. For instance, the Pacific Ocean, being the largest ocean basin, exhibits key climate modes such as the El Niño Southern Oscillation (ENSO), and the Interdecadal Pacific Oscillation (IPO; Henley et al., 2015, 2017; Power et al., 1999; Folland et al., 2002). Among them, ENSO stands out as the strongest interannual climate mode in tropical Pacific Ocean and has substantial global impact. ENSO is commonly separated into two types based on the region of greatest anomalous activity: Eastern Pacific (EP) El Niño and Central Pacific (CP) El Niño. EP (CP) El Niño is characterized by eastern (central) tropical Pacific warming during its positive phase. On the other hand, the IPO is a multidecadal climate mode with SST anomalies that extend more broadly than ENSO into the subtropics. During the positive phase of the IPO, sea surface temperature warm in the tropical eastern and central Pacific, while the subtropical central and western Pacific experience cooling (Henley et al., 2015).

The Indian Ocean displays distinct climate modes, including the Indian Ocean Dipole (IOD; Saji et al., 1999; Webster et al., 1999), and Subsurface Dipole Mode (SDM; Sayantani



80

85

95



& Gnanaseelan, 2015; Mohapatra & Gnanaseelan, 2021). The IOD and SDM vary from interannual to decadal time scales, with IOD defined using tropical Indian Ocean SST, while SDM is defined based on thermocline depth and 500 m ocean heat content (OHC500). The IOD is characterised by contrasting warming and cooling in the western and southeastern equatorial Indian Ocean during its positive phase. The SDM is characterised by the southwestern Indian Ocean warming and eastern and central equatorial Indian Ocean cooling during its positive phase.

The Atlantic Ocean exhibits two main climate modes: the North Atlantic Oscillation (NAO; Hurrell et al., 2003; Hurrell & Deser, 2009) and the Atlantic Multidecadal Oscillation (AMO; Deser et al., 2010). The NAO is an atmospheric mode of variability characterised by fluctuations in the sea level pressure difference between the Icelandic Low and the Azores High. The AMO is an oceanic mode of multidecadal variability in North Atlantic SST, marked by uniform warming and cooling during warm and cold phases.

In the southern hemisphere, the Southern Annular Mode (SAM; Gong & Wang, 1999; Marshall, 2003) represents an important atmospheric mode of variability in sea level pressure and is characterised by the north-south movement of the westerly wind belt over the mid and higher latitudes. In its positive phase, the SAM is associated with lower pressure over Antarctica and stronger poleward-shifted westerlies. Overall, these climate modes are regionally based and defined by specific spatial patterns and time evolution.

These modes have a substantial impact on the global climate through oceanic and atmospheric channels across multiple timescales. They are responsible for internal changes in regional and global teleconnection processes, including key systems such as monsoon dynamics, Walker and Hadley circulation, ocean circulation, sea level, and heat content (Arblaster et al., 2002; Taschetto et al., 2015; Dong & McPhaden, 2017; IPCC, 2023; Mohapatra et al., 2023). These modes interact with each other, either amplifying or suppressing one another, thereby further influencing climate dynamics at both regional and global scales (IPCC, 2023; Meehl & Arblaster, 2012; Park et al., 2023).

1.3 Representation of climate modes in CMIP

Past research indicates that while the simulation of various climate modes has improved across successive CMIP generations, notable biases remain (Lee et al., 2021; Bracegirdle et al., 2020; Fasullo et al., 2020; Flato et al., 2013; Coburn & Pryor 2021). Most CMIP5 models reproduce the AMO spatial pattern (Chen et al., 2018) but underrepresented low-frequency hemispheric teleconnections (Kavvada et al., 2013). Based on historical simulations, CMIP6 exhibits clear advances, for instance, improved representation of several ENSO characteristics,



105

110

115

120

125

130



more realistic IOD spatial patterns, and better reproduction of AMO variability, yet persistent issues remain, such as biases in IOD amplitude and weak coupling between near-surface and subsurface processes for ENSO (Planton et al., 2021; McKenna et al. 2020).

To better evaluate these natural climate patterns, piControl simulations provide longterm datasets of unforced climate variability, offering a stable baseline for the assessment of climate modes. By comparing CMIP6 outputs with observations and across models, these datasets enable systematic validation of climate modes, quantification of individual model limitations.

1.4 Objective of climate mode datasets from CMIP6

Many analyses in climate science require information on climate modes, for example, when assessing their impacts, conducting attribution studies, or investigating mode dynamics. It is often useful to have information on the modes uncontaminated by a global warming signal. However, these piControl outputs are large datasets and processing times can be long, especially for metrics such as subsurface temperature. To address this need, we provide an open dataset along with a detailed description of the derivation of eight key climate modes (EP-El Niño, CP-El Niño, IPO, IOD, SDM, AMO, NAO, and SAM) based on 23 CMIP6 piControl simulations and observations. Section 2.1 outlines the datasets used to derive these climate modes, including details of the CMIP6 models and observational products. Section 2.2 describes the methodologies adopted and the standard definitions employed to identify the climate modes and techniques adopted for validation. Section 3 presents the technical validation and quality control of the derived datasets, providing a detailed discussion of the spatial and temporal structures of the eight climate modes, highlighting their consistency and limitations when compared with observational data. Section 4 summarizes the key dataset characteristics and findings. Section 5 highlights the utility of climate modes indices, and outlines their potential applications for studying internal climate variability and supporting future climate assessments. Finally, section 6 provides the data availability statement for derived and original datasets.

2 Data and Methods

2.1 Data Description

Monthly CMIP6 sea surface temperature (SST; variable: tos), sea level pressure (SLP; variable: psl), and potential temperature (variable: thetao) are obtained from the Earth System Grid Federation (https://esgf-node.llnl.gov/projects/cmip6). The present study considers 23 CMIP6 models. Only models with 500 or more years of piControl runs are considered to ensure robust statistics. This criterion ensures that the derived indices capture statistically robust



140

characteristics of internal climate variability, independent of externally forced signals. Each model contributes continuous monthly fields from the ocean and atmosphere components, allowing for consistent computation of climate mode indices.

The selected models represent a diverse range of modelling centres and configurations, encompassing different resolutions, parameterizations, and coupled components. This diversity provides a comprehensive basis for evaluating model consistency and spread in representing climate modes. Model details, including the originating centres, ocean-atmosphere resolutions, and total simulation lengths are listed in Table 1.

Model	Model Centres	Ocean Component	Atmospheric	Duratio
name		(Horizontal	Component	n
		Resolution)	(Horizontal	(years)
			Resolution)	
	~ !! ~			1000
CanESM5	Canadian Centre for Climate	NEMO3.4.1	CanAM5 (128*64)	1000
	Modelling and Analysis	(361*290)		
	(CCCma)			
HadGEM3-	UK Met Office Hadley	NEMO-HadGEM3-	MetUM-HadGEM3-	500
GC31-LL		GO6.0 (ORCA1 1°)	GA7.1 (192*144)	

EC-Earth3-	EC-Earth Consortium	NEMO3.6 (362*292)	IFS cy36r4	505
CC			(512*256)	
CMCC-	Centro Euro-Mediterraneo sui	NEMO3.6 (ORCA025	CAM5.3 (288 x 192)	500
CM2-SR5	Cambiamenti Climatici	0.25°)		
	(CMCC)	,		
CNRM-	Centre National de Recherches	NEMO3.6 (ORCA1	Arpege 6.3 (T127,	500
CM6-1	Météorologiques (CNRM-	1°)	150km)	
	CERFACS)	- ,	22 (2222)	
GISS-E2-1-	NASA Goddard Institute for	GISS Ocean (1°)	GISS-E2.1 (144 x	851
G	Space Studies		90)	
CMCC-	Centro Euro-Mediterraneo sui	NEMO3.6 (ORCA1	CAM5.4 (288*192)	500
ESM2	Cambiamenti Climatici	1°)		
	(CMCC)			
EC-Earth3	EC-Earth Consortium	NEMO3.6 (ORCA1	IFS cy36r4	501
		1°)	(512*256)	



E3SM1-0	U.S. Department of Energy	MPAS-Ocean v6.0	E3M v1.0 C90	500
	(DOE)	(resolution 60 km to		
		30 km)		
MIROC6	JAMSTEC, AORI, NIES	COCO4.9 (360*256)	CCSR AGCM	800
	(Japan)		(256*128)	
MRI-ESM2-	Meteorological Research	MRI.COM4.4 2	MRI-AGCM3.5	500
0	Institute (MRI)	(360*364)	(320*160)	
HadGEM3-	UK Met Office Hadley Centre	NEMO-HadGEM3-	MetUM-HadGEM3-	500
GC31-MM		GO6.0 (ORCA025	GA7.1 (432*324)	
		0.25°)		
BCC-	Beijing Climate Center (BCC)	MOM4 (1°)	AGCM3 (T106, 46)	600
CSM2-MR				
IPSL-	Institute Pierre-Simon Laplace	NEMO3.6 (362*332)	LMDZ (144 * 143)	2000
CM6A-LR	(IPSL)			
MPI-ESM1-	Max Planck Institute for	MPIOM1.6.3	ECHAM6.3	500
2-HR	Meteorology (MPI-M)	(802*404)	(384*192)	
ACCESS-	ACCESS, CSIRO (Australia)	GFDL-MOM5	HadGAM2	1000
ESM1-5		(360*300)	(192*145)	
ACCESS-	ACCESS, CSIRO (Australia)	GFDL-MOM5	HadGEM3-GA7.1	500
CM2		(360*300)	(N96)	
CESM2	National Center for	POP2 (320*384)	CAM6 (288*192)	1200
	Atmospheric Research (NCAR)			
GFDL-CM4	NOAA Geophysical Fluid	GFDL-MOM6	GFDL-AM4.0.1	500
	Dynamics Laboratory (GFDL)	(1440*1080)	(360*180)	
CIESM	Chinese Academy of	CIESM-OM	CIESM-AM	500
	Meteorological Sciences	(720*560)	(288*192)	
FGOALS-g3	Institute of Atmospheric	LICOM3.0 (360*218)	GAMIL2 (180*90)	700
	Physics, Chinese Academy of			
	Sciences (IAP-CAS)			
SAM0-	Seoul National University	POP2 (320*384)	CAM5.3 with	700
UNICON	(SNU)		UNICON (320*384)	
CNRM-	Centre National de Recherches	NEMO3.6 (e-	Arpege 6.3 (T127)	500
ESM2-1	Météorologiques (CNRM- CERFACS)	ORCA1 1°)		

Table 1. List of CMIP6 model with their organisation.

150

155

160

165

170



Observation and reanalysis datasets are used for validating the climate modes. Monthly SST data is taken from Extended Reconstructed SST version5 (ERSSTv5) for the period 1900-2023. The latest version of ERSSTv5 incorporates updated datasets, including SST from ICOADS Release 3.0, Argo floats (above 5 m), and sea-ice concentration from HadISST2. It improves spatial and temporal variability by refining Empirical Orthogonal Teleconnections (EOTs) and correcting ship SST biases using buoy-based references and an unadjusted firstguess approach. The detailed description of ERSSTv5 is provided by Huang et al. (2017). The present study also considers the monthly potential temperature data from the Ocean Reanalysis System 5 (ORAS5) during 1958-2018. ORAS5 adopts 3DVar-FGAT mode with ensemble based bias correction scheme. Observations from satellite instruments and in-situ measurements like CTD, Mooring etc. are assimilated into the Nucleus for European Modelling of the Ocean versions 4.0 (NEMO4) ocean model (Zuo et al. 2018). Our study includes the monthly Sea level pressure data from ERA5 reanalysis product for the period 1940-2023. ERA5 is the 5th generation reanalysis project from the European Centre for Medium-Range Weather Forecasts (ECWMF). ERA5 is produced using 4D-Var data assimilation and model forecasts in CY41R2 of the ECMWF Integrated Forecast System (IFS) (Hersbach et al. 2020). The dataset incorporates updated analyses of sea-surface temperature, sea-ice concentration, and multiple observational records using an ocean-wave optimal interpolation scheme, providing global hourly/monthly data since 1940 at \sim 31 km (0.5° \times 0.5°) resolution, along with uncertainty estimates to assess data quality and reliability.

Using the above datasets, we derived eight climate modes in NetCDF format. All files, together with the generating codes, are publicly archived on Zenodo (Mohapatra et al. 2025; https://doi.org/10.5281/zenodo.17337105). Detailed descriptions of the data processing steps, including preprocessing, statistical derivation, and consistency checks, as well as a comprehensive evaluation against observational and reanalysis datasets, are provided in the Methodology and Technical Validation sections.

2.2 Methodology

As the first step, all observational, reanalysis, and CMIP model datasets were regridded to a $1^{\circ} \times 1^{\circ}$ grid using bilinear interpolation before any further processing.

2.2.1 Ocean Heat Content

The 500m upper Ocean Heat Content (OHC500) in reanalysis and models is computed as follows:

175
$$OHC500 = \rho_0 C_p \int_0^{500} T(z) dz$$



185

190

195

200

205



where Cp=4186 J Kg⁻¹ K⁻¹ is the specific heat capacity of the sea water and ρ_0 =1026 kg m⁻³ is the reference sea water density, T(z) is the vertical profile of regridded potential temperature.

2.2.2 Drift correction

Variables from piControl simulations, that are not subject to transient forcing, should be stationary over time. However, a common issue in climate models is the drift. Drift is a spurious trend in different state variables that are unrelated to changes in external forcing (Sen Gupta et al. 2013). Drift may occur for various reasons such as insufficient spin up and errors in the model's energy budget (Hobbs et al. 2016). This shortcoming in the models when integrated over century scales can result large changes in ocean temperature, and ocean heat content etc (Sen Gupta et al. 2013; Hobbs et al. 2016). To remove model drift, a linear trend was fitted and removed at each grid cell over the full duration of the piControl simulations for regridded SST, OHC500, and SLP.

2.2.3 Climate modes

We have calculated eight widely used climate modes (IPO, EP and CP El *Ni*ño, AMO, NAO, IOD, SDM, and SAM), using standard definitions of these modes in the literature (Table 2). First, monthly anomalies are calculated by subtracting the long-term (duration of piControl) monthly mean climatology from the SST, SLP, and OHC500, after the data had already been regridded and linearly detrended as described above.

A Lanczos filter was applied to the above processed datasets prior to computing the AMO, ENSO and IPO indices. For the AMO and IPO, a 10-year low-pass filter with a 10-year cut-off and a filter length of 121 months was used, which removes approximately five years of data from the beginning and end of the record. For ENSO, a band-pass filter with lower and upper cut-offs at 24 months and 108 months respectively, and a filter length of 109 months, was applied. The Lanczos filters (low-pass and band-pass) were chosen to retain only the desired frequency ranges required for defining climate mode (AMO, ENSO and IPO). To maintain consistency, we removed five years from the start and end of the record used for computing each of the climate mode index (Table 2). While the AMO is defined as the average of 10year low pass filtered SST anomaly over the North Atlantic as preferred in most literature, the other seven climate modes are defined based on Empirical Orthogonal Function (EOF) and applied separately to different regions/variables (as mentioned in Table 2).

EOF analysis decomposes spatiotemporal data into orthogonal spatial patterns and corresponding temporal coefficients, known as principal components (PCs), ranked by the variance they explain (Hannachi et al., 2007). We have not included the Niño 3.4 (for ENSO), DMI (Dipole Mode Index for IOD) indices in this study because they rely on specific, small-



area averages. Since models have biases in accurately representing these regions, we instead use EOF based PCs as indices, which better account for regional biases while capturing variability across the full basins.

Index	Definition	
AMO (Atlantic	Average of 10 years low pass filtered detrended monthly SST Anomaly average	
Multidecadal Oscillation)	over the North Atlantic (0-60°N,75°W-7.5°W)	
	(Enfield et al. 2001; Wang et al. 2009; Deser et al. 2021)	
IPO (Interdecadal Pacific	1st EOFPC of 10 years low pass filtered detrended monthly SST anomaly averaged	
Oscillation)	over the Pacific Ocean (70°S-70°N, 120°E-80°W). (Dong and McPhaden 2017;	
	Han et al. 2014; Power et al. 1999)	
El Niño (EP El Niño and	1st and 2nd EOFPC of 2-9 years band pass filtered detrended monthly SST anomaly	
CP El Niño)	over the tropical Pacific Ocean (120°E-80°W, 30°S-30°N). EOFPC1 (EOFPC2)	
	represents EP El Niño (CP El Niño). (Xu et al 2017)	
	Here EP El Niño is denoted as ENSO1 and CP El Niño is denoted as ENSO2.	
SAM (Southern Annular	1st EOFPC of detrended monthly sea level pressure anomaly south of 20°S (Cai	
Mode)	and Cowan 2007; Miller et al. 2006)	
NAO (North Atlantic	1st EOFPC of detrended monthly sea level pressure anomaly over the North	
Oscillation)	Atlantic Ocean (90°W-40°E,20°N-80°N) (Hurrel et al. 2003; Hurrel & Deser 2009)	
SDM (Subsurface Dipole	1st EOFPC of detrended monthly upper 500m OHC anomaly over the tropical	
Mode)	Indian Ocean (40°E-110°E, 20°S-25°N) (Mohapatra & Gnanaseelan, 2021)	
IOD (Indian Ocean	2 nd EOFPC of detrended monthly SST anomaly over the tropical Indian Ocean	
Dipole)	(40°E-110°E, 20°S-25°N). (Krishnamurthy & Kirtman, 2003)	

Table 2. Definition of various regional climate modes and their domains.

2.2.4 Model Skill score

215

220

225

To compare the spatial patterns of climate modes extracted from CMIP6 models with those from observations, we have employed Taylor diagrams. Taylor diagrams provide a concise visual representation of the spatial correlation coefficient (r) and the standard deviation (STD) between a model field and an observed field, while also incorporating their combined measure, the root-mean-square difference (RMSD) (Izzaddin et al., 2024; Taylor, 2001). The RMSD is calculated as:

$$RMSD^2 = \sigma_m^2 + \sigma_r^2 - 2 \sigma_m \sigma_r r$$

Where σ_m and σ_r are the standard deviations of the model and observed patterns, respectively, and r is their spatial correlation coefficient.

In our analysis, the model results were standardised relative to observation. This allows the distance from each model point to the reference (observed) point on the diagram to directly indicate the overall agreement between the simulated and observed spatial patterns.



240

245

250

255

2.2.5 Spectral analysis and Monte Carlo significance test

We analysed the periodic variability of the climate mode indices time series using the Fast Fourier Transform (FFT) and tested the statistical significance of spectral peaks via Monte Carlo simulation. For each time series, the mean was removed, and the series was normalised to unit variance before spectral estimation. The power spectrum was computed using the variance-normalised periodogram with a Hanning window and normalised such that.

$$\sum_{k=1}^{K} P(f_k) = 1$$

Where $P(f_k)$ is the power at frequency f_k , and K is the number of positive frequency bins.

To construct the null distribution, we fitted a first-order autoregressive (AR(1)) model to each series by estimating its lag-1 autocorrelation coefficient α (Wilks, 2011). A total of 1000 Monte Carlo time series were generated with the same length as the original data following the approach of Schulz & Mudelsee (2002):

$$x_t = \alpha x_{t-1} + \varepsilon_t, \quad \varepsilon_t \sim \mathcal{N}(0,1)$$

The FFT is applied to each surrogate, and the resulting simulated spectra are used to estimate the mean $\overline{P}(f)$, standard deviation $\sigma_P(f)$, and the effective degrees of freedom (EDF) at each frequency (Bretherton et al., 1999):

$$EDF(f) = \left[\frac{\overline{P}(f)}{\sigma_P(f)}\right]^2$$

The significance threshold at each frequency was then calculated as

$$T(f) = \overline{P}(f) + \frac{\sigma_P(f)}{\sqrt{\text{EDF}(f)}}$$

And peaks in the observed spectrum exceeding this threshold (mean + standard error) are considered statistically significant. This procedure is repeated for all CMIP6 models, observational and reanalysis datasets to assess the robustness of periodic signals in the extracted climate mode indices. For the heat maps, we plot the fraction of significant spectral power in each period bin for every dataset. Within each dataset, these fractions are normalized to sum to 1 (i.e., we condition on the significant part of the spectrum), so the heat map reflects the relative distribution of significant power across periods rather than absolute magnitude. Bins with no significant power are left blank.

3 Technical Validation

3.1 Spatial and Statistical Quality Control of Simulated Climate Modes

3.1.1 Pacific Ocean Basin



265

270

275

3.1.1.1 ENSO (EP El Niño and CP El Niño)

The tropical Pacific Ocean exhibits a dominant interannual climate mode known as El Niño Southern Oscillation, comprising of two types of EP and CP El Niño. These two types of modes are defined as the first two leading modes of SST anomaly in the tropical Pacific within 30°S-30°N (Xue et al. 2017). The EP El Niño represents the primary leading mode and is characterized by warming in the eastern tropical Pacific and explains 63.4% of the variance of tropical Pacific SST anomaly in observation (Fig. 1a). Spatial expression, obtained by regressing SST anomaly against the normalised time series of mode indices (EOFPC1) show that most models capture the broad scale features, particularly warming in the eastern and central tropical Pacific Ocean during its positive phase (Fig. 1a). All the models reproduce the observed wedge-shaped warming in the central and eastern Pacific, with a weaker cooling signal in the surrounding regions. Pattern correlations range between 0.7 to 0.95 with RMSE error ranging between 0.35°C to 0.55°C (Fig. 4a). Models (particularly CanESM5, BCC-CSM2-MR, IPSL-CM6A-LR, ACCESS-ESM1.5, and SAM0-UNICON) present warming signal that extends too far to the west along the equator and show maximum anomalies too far to the west. Despite these limitations, all the models broadly replicate the observed spatial pattern, with RMSE values around 0.5°C.

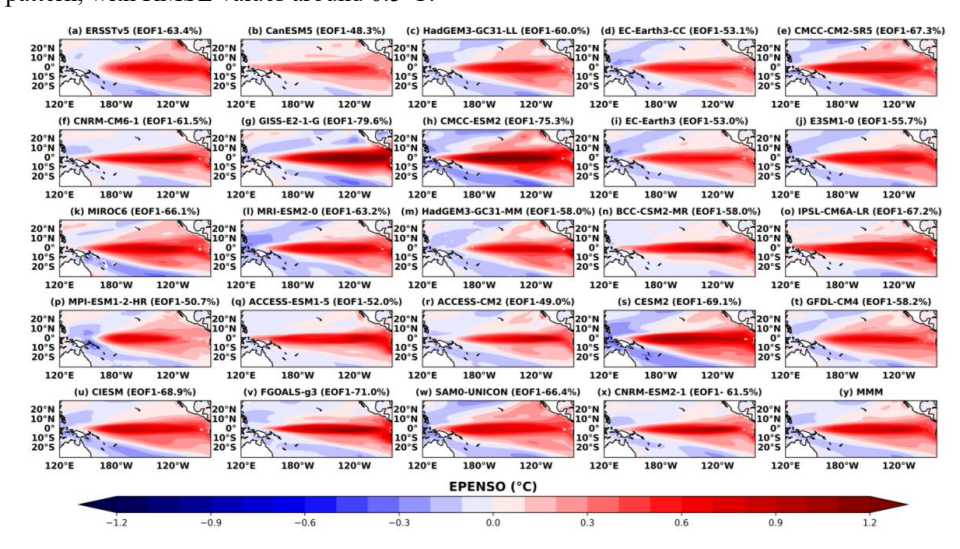


Fig. 1 Spatial pattern of regression-derived ocean response for the Eastern Pacific El Nino (EP El Nino: ENSO1). Values are sea surface temperature (2-9year band pass filtered) anomalies (in °C) regressed against the EOFPC (ENSO1) time series from (a) ERSSTv5, (b-x) 23 CMIP6 models and (y) MMM. Here MMM represents the average of spatial pattern of regression from 23 CMIP6 models. The





285

290

295

bracketed text and numbers in black are the mean variance explained by the EOF representing ENSO1 between observations and models.

Unlike the EP El Niño, models demonstrate a large inter-model spread in representing the observed warming in the central Pacific expanding to lower latitudes towards the east and with cooling in the eastern and western tropical Pacific Ocean which are the characteristics of the positive phase of CP El Niño (Fig. 2, Fig. 4b). This mode explains only 8.1% of the variance in the observation, which is much less than the EP El Niño. Similarly low variances are seen across the models varying between 5%-15% (Fig. 2). With respect to observation, 14 out of 23 models have correlations that exceed 0.5, whereas 6 models show lower correlations in between 0.2-0.5 and 2 models (CESM2 and CIESM) show negative correlation (Fig. 4b). Models such as CanESM5, CMCC-CM2-SR5, BCC-CSM2-MR, ACCESS-ESM1-5 and MIROC6 show the central Pacific warming extending into the western Pacific, whereas EC-Earth3-CC, E3SM1-0, CESM2, and CIESM display warming in the central and eastern Pacific, which deviates from the conventional CP El Niño spatial features, as indicated by RMSE values exceeding 1°C. These deviations are likely due to the smaller variance associated with this mode. Despite these issues, the MMM effectively captures the observed climate mode by reducing non-systematic biases coming from individual models and a lower RMSE of around 0.5°C (Fig. 4b).

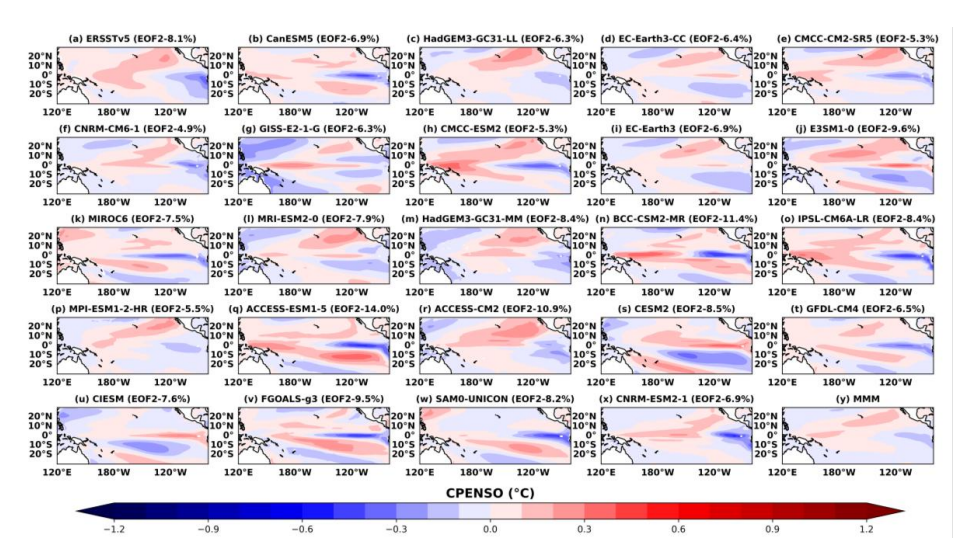


Fig. 2 Spatial pattern of regression-derived ocean response for the Central Pacific El Nino (CP El Nino: ENSO2). Values are sea surface temperature (2-9 years band pass filtered) anomalies (in °C) regressed against the EOFPC (ENSO2) time series from (a) ERSSTv5, (b-x) 23 CMIP6 models and (y) MMM. Here MMM represents the average of spatial pattern of regression from 23 CMIP6 models. The

https://doi.org/10.5194/essd-2025-618 Preprint. Discussion started: 11 November 2025 © Author(s) 2025. CC BY 4.0 License.



305

310

315



bracketed text and numbers in black are the mean variance explained by the EOF representing ENSO2 between observations and models.

3.1.1.2 Interdecadal Pacific Oscillation (IPO)

The IPO is a multidecadal climate mode and captured as the first leading mode of variability in low frequency SST anomaly in the Pacific Ocean (Dong and McPhaden 2017; Han et al. 2014; Power et al. 1999), accounting for 32.3% of variance in observation (Fig. 3a). However, for EC-Earth3 and HadGEM3-GC31-LL, IPO appears as the second and third leading modes of SST, respectively (Fig. 3c, i), as indicated by the corresponding EOFs that show strong correlations with the observed IPO spatial pattern. In most CMIP6 models, the IPO explains 25–35% of the variance, consistent with observations, though models such as CNRM-CM6-1, GISS-E2-1-G, FGOALS-g3, and CNRM-ESM2-1 show lower values (<20%), while CESM2 shows higher variance (44%). The observed IPO pattern exhibits a characteristic tripolar structure with warming in the central to eastern tropical Pacific and cooling in the western-central North and South Pacific, corresponding to the positive phase of the IPO (Fig. 3a).

325

330

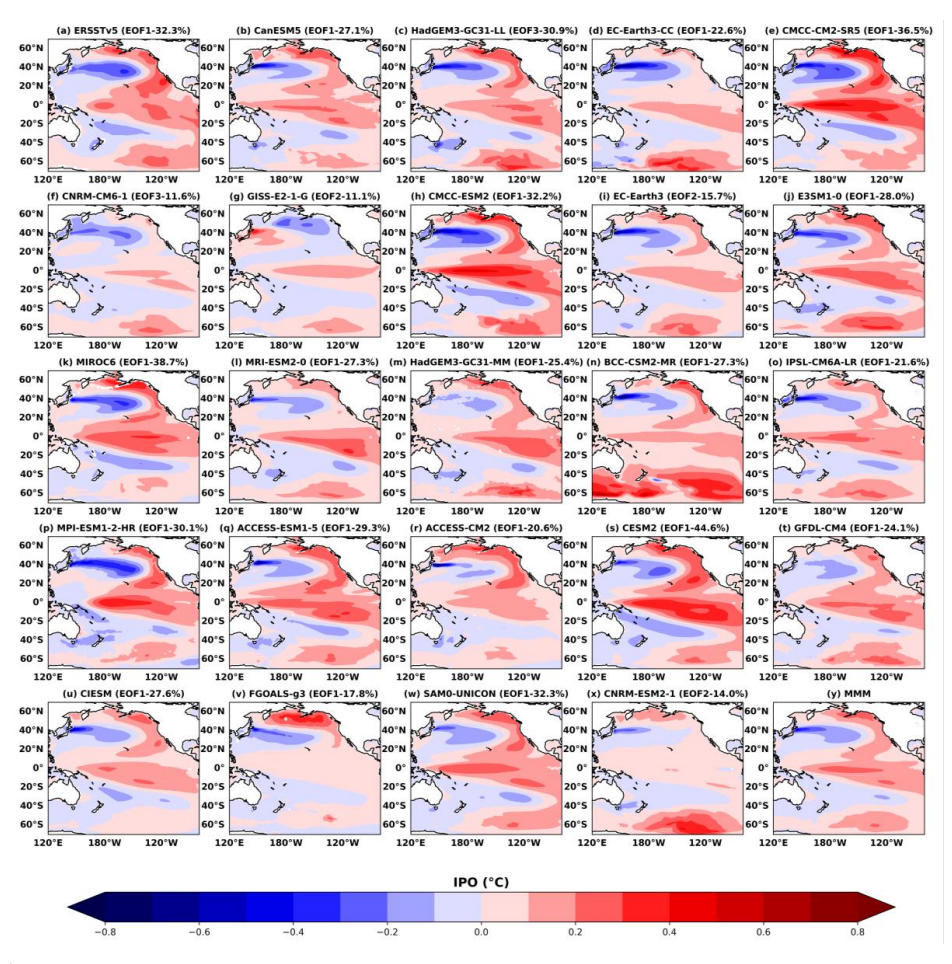


Fig. 3 Spatial pattern of regression-derived ocean response for the Interdecadal Pacific Oscillation (IPO). Values are sea surface temperature (10year low pass filtered) anomalies (in °C) regressed against the EOFPC (IPO) time series from (a) ERSSTv5, (b-x) 23 CMIP6 models and (y) MMM. Here MMM represents the average of spatial pattern of regression from 23 CMIP6 models. The bracketed text and numbers in black are the mean variance explained by the EOF representing IPO between observations and models.

To examine the robustness of spatial pattern, we have calculated the spatial correlation between the observed and modelled IPO pattern (Fig. 4c), revealing that 19 CMIP6 models exhibit strong correlations ranging from 0.7 to 0.9, with low RMSE around 0.5°C. However, most models simulate the characteristic warming in the equatorial eastern Pacific extending westward, though with varying amplitudes compared to observation. For example, GISS-E2-1-G simulates positive anomalies over the western North Central Pacific (Fig. 3g), in contrast to the observed negative anomalies. Similarly, BCC-CSM2-MR shows basin-wide warming



across the South Pacific (Fig. 3n). Overall, the MMM reproduces the IPO spatial pattern and variance reasonably well, demonstrating robust representation of the observed low-frequency Pacific variability.

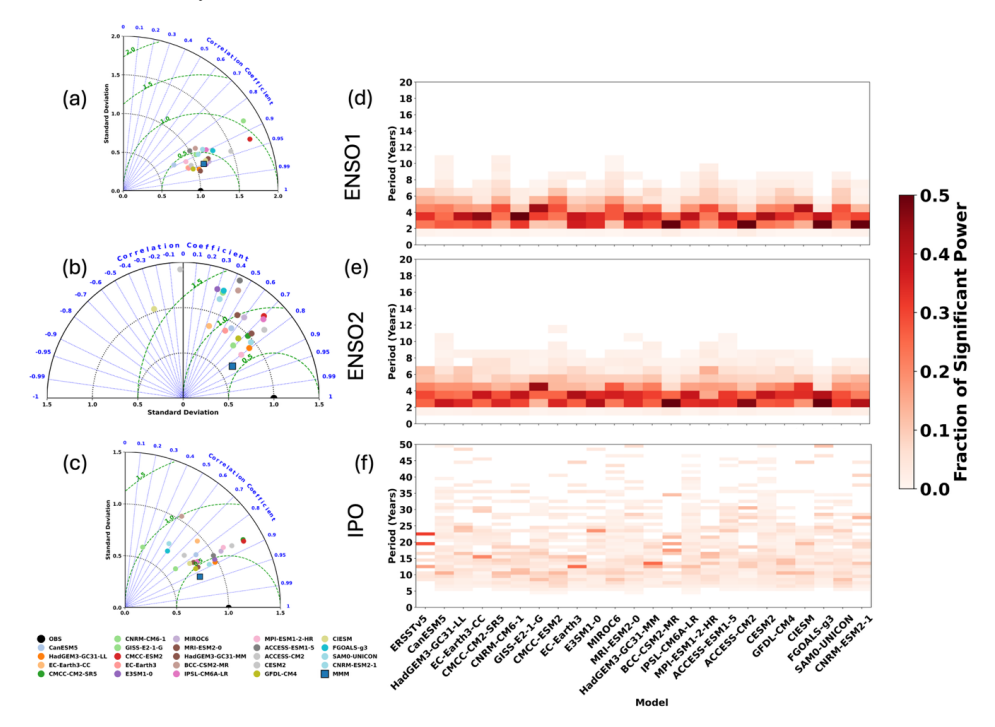


Fig. 4 Taylor diagram for regression based spatial pattern of (a) ENSO1 (b) ENSO2 (c) IPO from observation, 23 CMIP6 models and MMM. (d, e, f) Power spectrum of normalised time series for (d) ENSO1, (e) ENSO2 and (f) IPO climate mode indices from observation and 23 CMIP6 models. The power is plotted for values above a threshold (mean + standard error) after performing power analysis using a Monte Carlo-based significance test.

3.1.2 Indian Ocean basin

335

340

345

3.1.2.1 Indian Ocean Dipole (IOD)

The IOD, an internal mode of variability in tropical Indian Ocean SST, is characterised by warming (cooling) in the WEIO (EEIO) during its positive phase (Krishnamurthy and Kirtman 2003; Saji et al. 1999). Most models represent the IOD as the second leading mode of variability in SST anomaly, while 7 models (CMCC-CM2-SR5, BCC-CSM2-MR, ACCESS-ESM1-5, CESM2, CIESM, FGOALS-g3, SAM0-UNICON) exhibit the IOD as 1st leading mode (Fig. 5). Observed IOD accounts for 12.7% of the total SST anomaly variance in the tropical Indian Ocean (Fig. 5a). The explained variance in CMIP6 models varies widely, from





355

360

9.5% (CanESM5) to 31.5% (CIESM), while 8 models explains within the observed range of 10%-15%. A strong agreement exists between the simulated and observed spatial patterns of the IOD, with pattern correlations ranging from 0.4 to 0.9 across all the models (as shown in Taylor diagram in Fig. 7a), though notable regional differences remains in reproducing the magnitude of warming and cooling over the western and eastern IO. For instance, a subset of seven models (CMCC-ESM2, EC-Earth3-CC, EC-Earth3, E3SM1-0, CIESM, MIROC6, and SAM0-UNICON) simulates strong cooling over Java and Sumatra region, resulting in high RMSE ranging between 1.0 and 1.5°C. Conversely, models like CMCC-CM2-SR5 and CESM2 produce exaggerated warming in the western IO. The MMM mitigates these individual model biases and achieves a closer representation of the observed IOD spatial pattern, demonstrated by a strong pattern correlation (0.7) and a substantially lower RMSE (0.6°C).

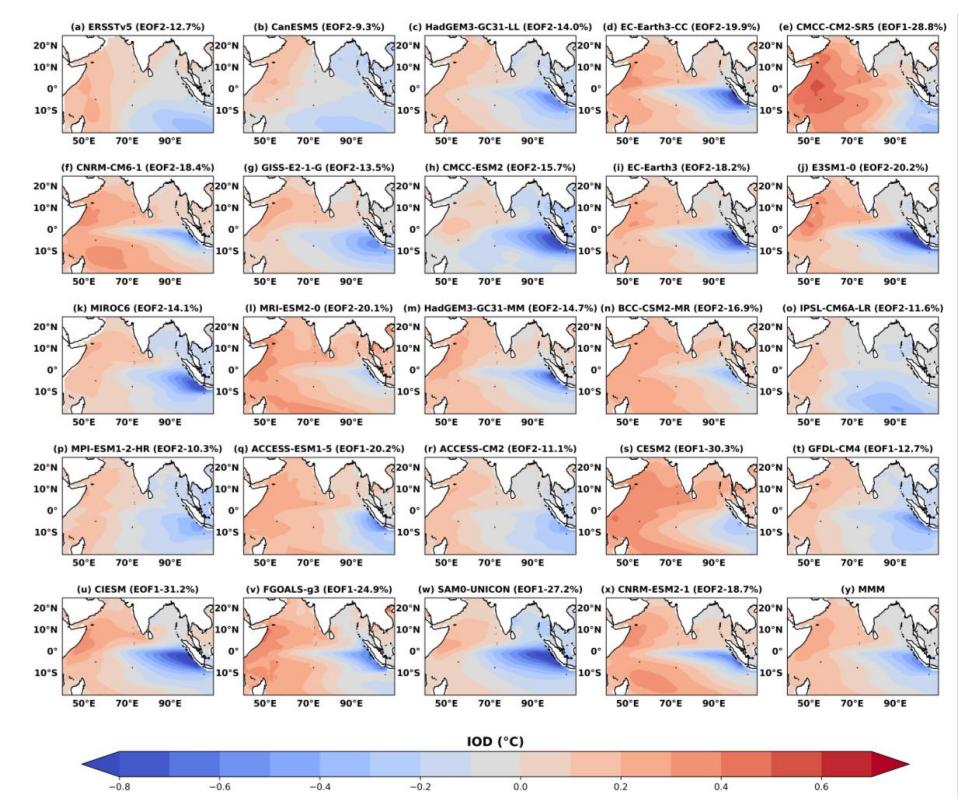


Fig. 5 Spatial pattern of regression-derived ocean response for the Indian Ocean Dipole (IOD). Values are sea surface temperature anomalies (in °C) regressed against the EOFPC (IOD) time series from (a) ERSSTv5, (b-x) 23 CMIP6 models and (y) MMM. Here MMM represents the average of spatial pattern of regression from 23 CMIP6 models. The bracketed text and numbers in black are the mean variance explained by the EOF representing IOD between observations and models.



375

380

3.1.2.2 Subsurface Dipole Mode (SDM)

The SDM is an internal mode of variability in the upper 500m OHC of the tropical Indian Ocean, characterised by a distinct dipolar pattern with warming in the south-western Indian Ocean (SWIO) and cooling in the EEIO during its positive phase (Mohapatra and Gnanaseelan 2021). All 23 models, along with reanalysis data (ORAS5), represent the SDM as the dominant EOF in OHC500 anomaly (Fig. 6). Reanalysis data accounts for 21% of the total variance. The explained variance in CMIP6 models varies widely from 14.4% in HadGEM3-GC31-MM to over 40% in CIESM and FGOALS-g3. The SDM pattern in reanalysis shows warming (cooling) in the SWIO (EEIO) (Fig. 6a). Most models reproduce the observed SWIO and EEIO dipole structure of SDM, though a few models underestimate the observed warming over the Arabian Sea (Fig. 6).

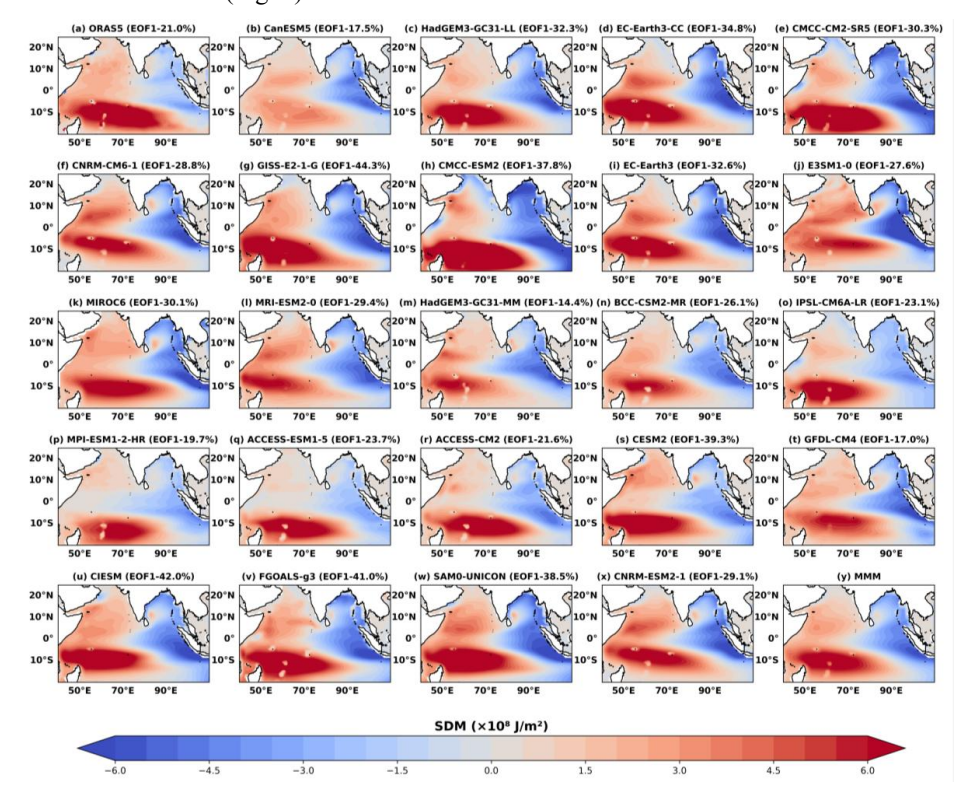


Fig. 6 Spatial pattern of regression-derived ocean response for the Subsurface Dipole Mode (SDM). Values are sea surface temperature anomalies (in *10⁸ J/m²) regressed against the EOFPC (SDM) time series from (a) ORAS5, (b-x) 23 CMIP6 models and (y) MMM. Here MMM represents the average of spatial pattern of regression from 23 CMIP6 models. The bracketed text and numbers in black are the mean variance explained by the EOF representing SDM between observations and models.



390

395

400

405

All the models exhibit a strong correlation with reanalysis, ranging from 0.6 to 0.9 (Fig. 7b). The majority of models also display low RMSE values, around 0.5*10⁸ J/m². In contrast, CMCC-ESM2 exhibits a notably higher RMSE, exceeding 1*10⁸ J/m² (Fig. 7b), primarily due to its exaggerated amplitude in the SWIO relative to reanalysis (Fig. 6b). Overall, the CMIP6 models demonstrate good skill in capturing the SDM's spatial characteristics, underscoring their ability to represent key OHC variability in the tropical Indian Ocean.

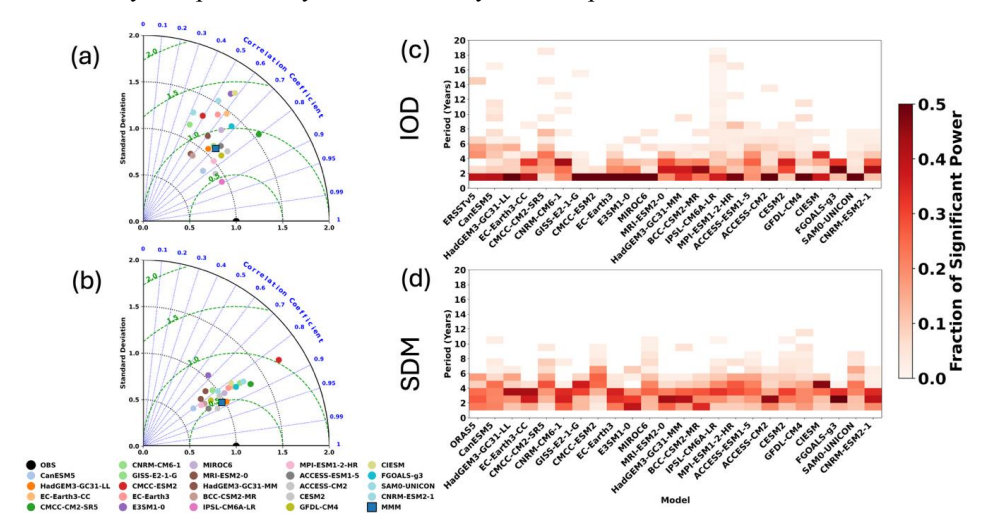


Fig. 7 Taylor diagram for regression based spatial pattern of (a) IOD from ERSSTv5 (b) SDM from ORAS5, 23 CMIP6 models and MMM. (c, d) Power spectrum of normalised time series for (c) IOD and (d) SDM climate mode indices from observation and 23 CMIP6 models. The power is plotted for values above the threshold (mean + standard error) after performing power analysis using a Monte Carlo-based significance test.

3.1.3 Atlantic Ocean basin

3.1.3.1 Atlantic Multidecadal Oscillation (AMO)

The AMO is an important multidecadal oceanic climate mode in the North Atlantic Ocean, characterised by basin-wide warming in the North Atlantic Ocean (Fig. 8a). All the models display the large-scale features of the observed AMO pattern (Fig. 8), through several show regional deviations. 10 out of the 23 models (EC-Earth3-CC, GISS-E2-1-G, EC-Earth3, E3SM1-0, MIROC6, MRI-ESM2-0, GFDL-CM4, FGOALS-g3, SAM0-UNICON, CNRM-ESM2-1) exhibit a cooling pattern in the western-central North Atlantic Ocean. Several models also show amplitude deviations from observation, particularly north of 40°N, where the warming is either stronger or weaker than observed. These differences are reflected in the broader correlation range (0.2 to 0.7) between the models and observation (Fig. 11a). For

example, eight models (EC-Earth3, CMCC-CM2-SR5, CMCC-ESM2, CNRM-ESM1-0, FGOALS-g3, CNRM-CM6-1, and IPSL-CM6A-LR) show excessive warming north of 40°N, while FGOALS-g3 exhibits strong cooling in the western-central North Atlantic with RMSE values exceeding 2°C, and even exceeding 6°C (for EC-Earth3) (Fig. 11d). The MMM effectively mitigates these discrepancies, providing a more consistent representation of the observed AMO pattern, with a correlation of 0.6 and RMSE below 2°C, demonstrating improved overall skill relative to individual models.

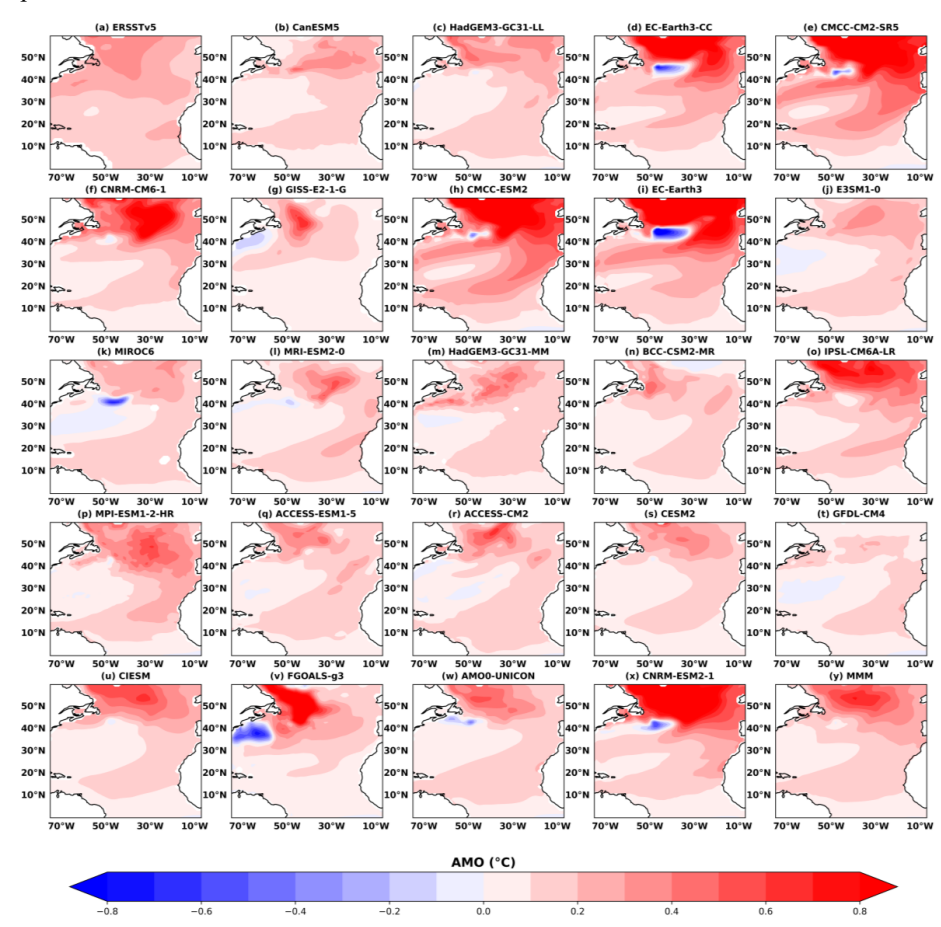


Fig. 8 Spatial pattern of regression-derived ocean response for the Atlantic Multidecadal Oscillation (AMO). Values are sea surface temperature (10year low pass filtered) anomalies (in °C) regressed against the AMO time series from (a) ERSSTv5, (b-x) 23 CMIP6 models and (y) MMM. Here MMM represents the average of spatial pattern of regression from 23 CMIP6 models.

3.1.4 Atmospheric Modes

420 3.1.4.1 North Atlantic Oscillation (NAO)

430

435

440

The NAO, an atmospheric mode of variability in SLP over the North Atlantic Ocean, is defined as a distinct north-south dipolar SLP pattern, with high (low) SLP anomaly in the north (south) of the North Atlantic Ocean during its positive phase (Hurrel et al. 2003; Hurrel & Deser 2009). Reanalysis (ERA5) and all 23 models represent the NAO as the leading mode of variability in SLP anomaly (Fig. 9). Reanalysis data explains 33.1% of the total variance, while models account 28%-35% in SLP anomaly, indicating a strong imprint of the NAO in atmospheric circulation over this region. Models successfully reproduce this canonical NAO spatial pattern with varying amplitude across the basin. All the models exhibit very strong spatial correlation (>0.95) with reanalysis and maintain very low RMSE values (< 5 Pa), underscoring the overall robustness and consistency of CMIP6 models in representing the observed NAO structure (Fig. 11b).

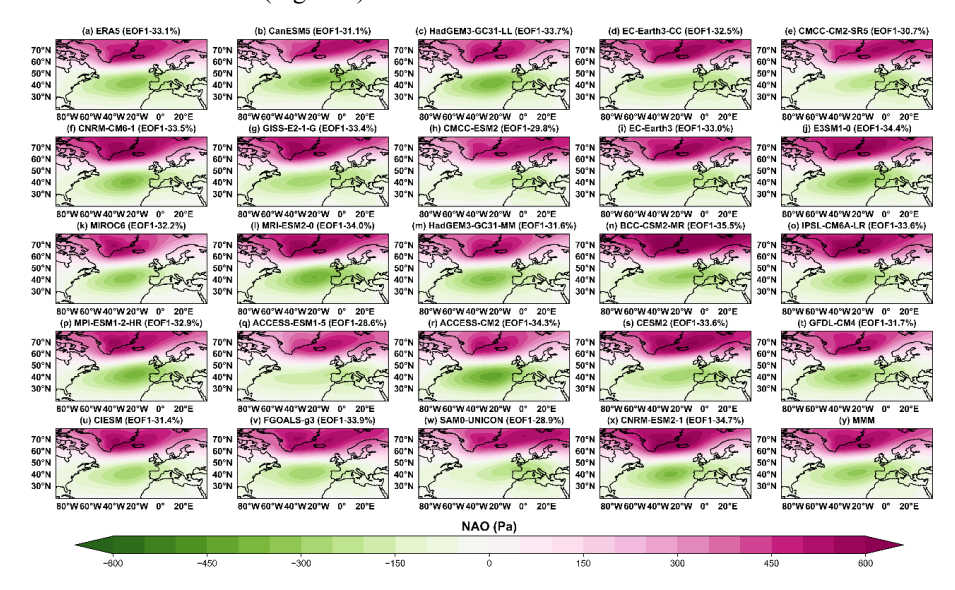


Fig. 9 Spatial pattern of regression-derived ocean response for the North Atlantic Oscillation (NAO). Values are sea level pressure anomalies (in Pa) regressed against the EOFPC (NAO) time series from (a) ERA5, (b-x) 23 CMIP6 models and (y) MMM. Here MMM represents the average of spatial pattern of regression from 23 CMIP6 models. The bracketed text and numbers in black are the mean variance explained by the EOF representing NAO between observation and models.

3.1.4.2 Southern Annular Mode (SAM)

The southern hemisphere extra-subtropics are dominated by an atmospheric mode known as the SAM, which is characterised by a north-south shift in westerly wind belts. Reanalysis (ERA5) and all CMIP6 simulations capture SAM as the primary climate mode in SLP anomaly. Reanalysis explains 26% of total variance, while models capture 26%–35%. The



regression based spatial pattern of the SAM shows negative SLP anomalies over the polar region and positive anomalies over the extra-subtropical latitudes, a feature reproduced by the models (Fig. 10). All models show strong correlation (>0.97) and low RMSE (<5 Pa) with reanalysis (Fig. 11c), confirming the robustness of SAM representation and the reliability of the CMIP6-derived SAM index for studying southern hemisphere climate variability.

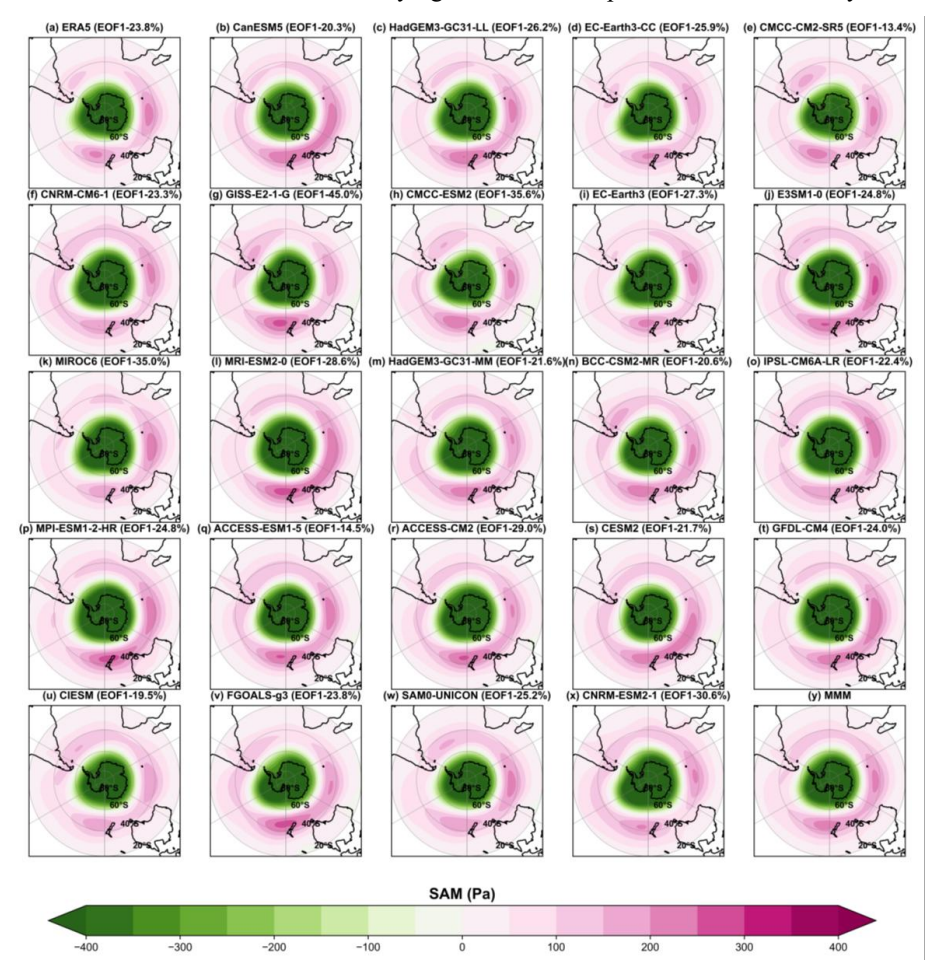


Fig. 10 Spatial pattern of regression-derived atmospheric response for the Southern Annular Mode (SAM). Values are sea level pressure anomalies (in Pa) regressed against the EOFPC (SAM) time series from (a) ERA5, (b-x) 23 CMIP6 models and (y) MMM. Here MMM represents the average of spatial pattern of regression from 23 CMIP6 models. The bracketed text and numbers in black are the mean variance explained by the EOF representing SAM between observation and models.

460

465

470

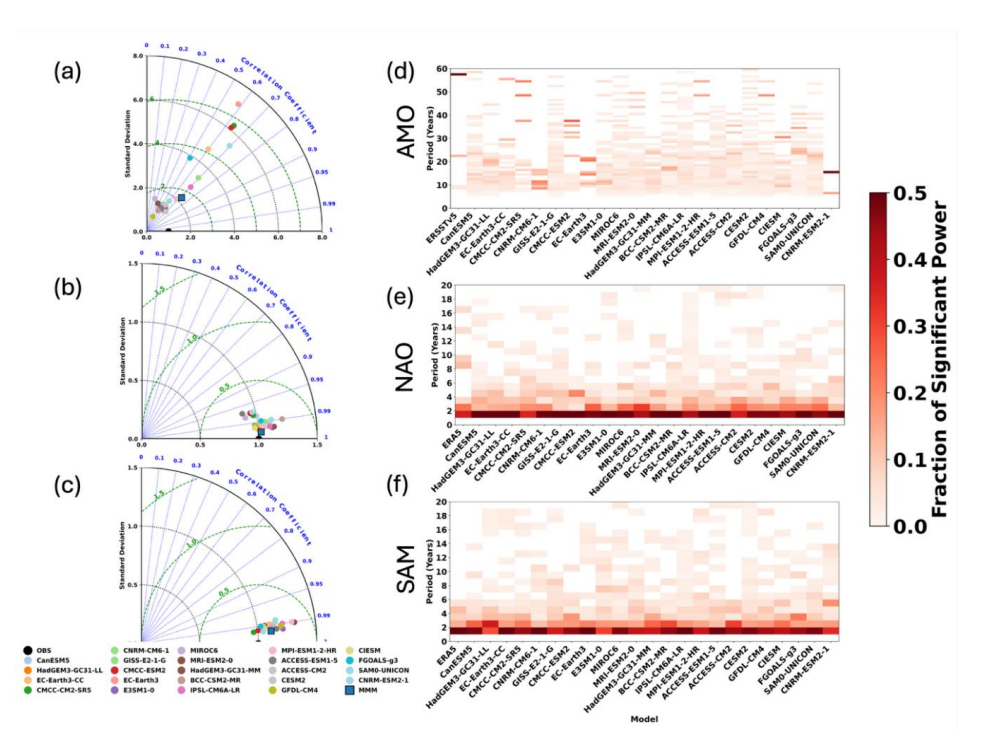


Fig. 11 Taylor diagram for spatial pattern (regression based) of (a) AMO (b) NAO, and (c) SAM in observation, 23 CMIP6 models and MMM. (d, e, f) Power spectrum of normalised time series for (d) AMO, (e) NAO and (f) SAM climate mode indices from observation and 23 CMIP6 models. The power is plotted for values above the threshold (mean + standard error) after performing power analysis using a Monte Carlo–based significance test.

3.2 Verification of Temporal Variability of Simulated Climate Modes

Following our examination and evaluation of the spatial patterns of climate modes, we also investigate their temporal structure. ENSO is the strongest climate mode, with a periodicity on interannual time scales ranging from 2–7 years (Xu et al. 2017). Both observed ENSO1 and ENSO2 show a clear periodicity between 2–7 years, which is broadly captured by all the models, though several extending beyond 7 years. The broader distribution of power in the models reflects their substantially longer simulation periods compared to the relatively short observational record. Notably, ENSO1 periodicity extends beyond 10 years in CanESM5, CMCC-CM2-SR5, and MIROC6, while for ENSO2, CanESM5, CMCC-ESM2, MRI-ESM2-0, and ACCESS-ESM1-5 show periodicities exceeding 10 years. Similarly, the observed IPO exhibits a multidecadal periodicity in the 10–30 years range (Fig. 4f). The models also capture this periodicity, though it extends beyond 30 years, and shows a greater number of significant power peaks than observations. In contrast, the extended model simulations show more



480

485

490

495

500

505



significant power, extending up to 50years reflecting their longer integration periods, but mostly concentrated within the 10-20 years range. Models such as CanESM5 (1000 years), MIROC6 (800 years), IPSL-CM6A-LR (2000 years), CESM2 (1200 years), that have long simulation lengths, exhibit a higher number of spectral peaks compared to other models.

The observed IOD shows periodicity at interannual time scale, with decadal fluctuations at 15 years (Fig. 7c). It exhibits strong power at Year 2, which is also reflected in most models. Models such as CanESM5, CMCC-CM2-SR5, IPSL-CM6A-LR, and MPI-ESM1-2-HR exhibit broader spectral power up to 20 years, whereas IPSL-CM6A-LR, with its 2000-year simulation, shows significant spectra over the entire 20 years period. For the SDM, the reanalysis (ORAS5) based index exhibits significant spectral power within 6 years (Fig. 7d), while models display this range with additional peaks extending up to 12 years. For instance, the periodicity of SDM extends beyond 10 years in CanESM5, IPSL-CM5A-LR, CESM2 and GFDL-CM4.

Spectral analysis of the observed AMO index indicates clear periodicity in the 10-60 years range (Fig. 11d) represented by three significant power peaks. The extended piControl simulations show a broader distribution of power across this range, with several significant peaks spread throughout. CNRM-CM6-1, EC-Earth3, CMCC-ESM2 and CNRM-ESM2-1 show comparatively fewer spectra than other models, with EC-Earth3 and CNRM-ESM2-1 showing peaks limited to 10-25 years range (Fig. 11d). For NAO, the reanalysis data exhibits a dominant spectral peak within 4 years, and more peaks scattered between 8 and 15 years, indicating variability spanning both interannual and decadal timescales (Fig. 11e). The Reanalysis shows strong power at the 2-year period, which gradually weakens but remains significant, a feature that is more prominent across all the models. Most models display significant spectral power concentrated within the 7-year range, with additional peaks unevenly distributed between 10 and 20 years (Fig. 11e).

The SAM shows a pronounced spectral peak within a 6-year period in the reanalysis, reflecting strong interannual variability (Fig. 11f). The reanalysis also indicates notable power at the 2-year period, which diminishes with increasing period yet remains statistically significant, a pattern consistently reproduced by the models. Across the CMIP6, most models exhibit dominant power beyond 6 years, with several displaying additional, unevenly distributed peaks between 6 and 20 years.

Overall, this temporal assessment demonstrates that CMIP6 models capture the observed periodicity and variability of major climate modes across interannual to multidecadal timescales. While differences remain in amplitude and spectral spread, the general agreement





across models, observations and reanalyses indicates a consistent and physically realistic representation of internal climate variability.

4 Conclusion

510

515

520

525

530

535

540

Here, we provide datasets for eight different climate modes (EP-El Niño, CP-El Niño, IPO, IOD, SDM, AMO, NAO, and SAM) from 23 CMIP6 piControl simulations. Our findings suggest that the spatial and temporal structures of these climate modes in the piControl simulations, spanning 500 to 2000 years, broadly resemble the observed patterns, with models showing higher skill in representing atmospheric modes than oceanic modes. However, there are notable differences in capturing the amplitude and regional structure of these modes due to the model resolution, missing physics, and inadequate parameterization. Although the models reproduce many key features seen in observations, the wide differences in their representation of CP El Niño and AMO highlight greater uncertainties compared to the other climate modes.

5 Data Usage

These standardised pre-processed datasets will allow researchers to bypass the time-consuming step of processing raw outputs, enabling them to focus on scientific inquiry and interpretation. The uniform definitions and methodologies embedded in this dataset ensure that analyses across different studies and climate models are comparable and consistent, fostering collaborative research and cross-validation of results. Moreover, it provides a crucial benchmark for evaluating climate model performance, helping identify limitations and guiding future improvements. This resource is potentially useful for detection and attribution studies, where distinguishing internal variability such as ENSO, SAM or IOD that alias into anthropogenic influences is essential for understanding short-term trends in observed climate records. These data products are suitable for exploring the influence of internal modes such as ENSO, SAM, and IPO on global and regional climate variability of sea level, and ocean heat content. By enabling robust statistical analysis and more precise attribution, these climate modes database can become a useful tool for both climate research and assessments informing IPCC reports and climate impact evaluations.

Furthermore, the dataset can serve as a benchmark for future climate model development and tuning, as it highlights both the strengths and limitations in simulating key climate modes. It also provides an empirical foundation for improving multi-model ensemble analyses, and long-term climate projections. The inclusion of associated scripts ensures transparency and allows users to extend or modify the analysis framework for their specific research needs.

6 Data Availability Statement



550

555

565



The resulting datasets, generated in NetCDF format, are publicly available via Zenodo (Mohapatra et al. 2025; https://doi.org/10.5281/zenodo.17337105). This includes EOFs, mode indices including PCs, normalised PCs and regression based spatial pattern files from 23 CMIP6 piControl simulations, observations and reanalysis. The Zenodo archive also contains the codes used to generate these datasets. The 23 CMIP6 model directory contains datasets that includes the spatial, temporal, and normalized temporal components of eight commonly examined climate modes. The Observation_Reanalysis directory provides equivalent datasets from observational and reanalysis products for comparison and validation. The Regression_Based_Spatial_Patterns directory includes regression-derived spatial patterns based on key variables such as sea surface temperature (SST), sea level pressure (SLP), and ocean heat content (OHC). The Codes directory contains the NCL and Ferret scripts that is used for data processing, EOF analysis, regression computation.

original CMIP6 monthly outputs available https://esgfare at node.llnl.gov/projects/cmip6. ERA5 Sea level data taken from pressure is https://cds.climate.copernicus.eu/cdsapp#!/dataset/reanalysis-era5-single-levels-monthlymeans?tab=overview and ERSSTv5 sea surface temperature data are provided by NOAA/PSL (https://downloads.psl.noaa.gov/Datasets/noaa.ersst.v5/). ORAS5 monthly temperature reanalysis data can be accessed from Asia-Pacific Data-Research Center (http://apdrc.soest.hawaii.edu/las/v6/dataset?catitem=16535).

560 Code Availability Statement

All the programming codes used in preparing figures in this study are publicly available and can be downloaded from https://github.com/sandeep801/ClimateMode-Analysis.git.

Author Contributions

SM, ASG and NLB conceived the idea and designed the study. SM carried out the work and derived all datasets, with ASG and NLB providing scientific input to refine the methodology and analysis. YL computed and prepared the Taylor diagram, and Power spectrum. SM wrote the first draft of the paper with inputs from ASG, NLB and YL. All authors contributed to improving the quality of the manuscript.

Competing Interests

570 The authors declare no personal, professional competing interests.

Acknowledgements

We thank University of Tasmania, Hobart and University of New South Wales, Sydney for the support. SM thanks the Australian Centre for Excellence in Antarctic Sciences (ACEAS), Australian Antarctic Program Partnership (AAPP). We acknowledge the Australia's National





575 computational Infrastructure (NCI) for the significant computational facilities and storage of datasets. All the data sources of various centres are duly acknowledged. Datasets and figures are prepared using Python, NCL and Pyferret.

Financial Support

This work has been supported by the Australian Centre for Excellence in Antarctic Science (ACEAS). This project also received grant funding from the Australian Government as part of the Antarctic Science Collaboration Initiative program.

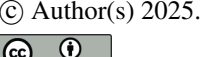
Reference

- Arblaster, J. M., Meehl, G. A., and Moore, A. M.: Interdecadal modulation of Australian rainfall, Clim. Dyn., 18, 519–531, https://doi.org/10.1007/s00382-001-0191-y, 2002.
- Bindoff, N. L., and Wunsch, C.: Comparison of synoptic and climatologically mapped sections in the South Pacific Ocean, J. Clim., 5, 631–645, https://doi.org/10.1175/1520-0442(1992)005<0631:COSACM>2.0.CO;2, 1992.
- Bracegirdle, T. J., Holmes, C. R., Hosking, J. S., Marshall, G. J., Osman, M. B., Patterson, M., and Rackow, T.: Improvements in circumpolar Southern Hemisphere extratropical atmospheric circulation in CMIP6 compared to CMIP5, Earth Space Sci., 7, 1–10, https://doi.org/10.1029/2019EA001065, 2020.
 - Bretherton, C. S., Widmann, M., Dymnikov, V. P., Wallace, J. M., and Bladé, I.: The effective number of spatial degrees of freedom of a time-varying field, J. Clim., 12, 1990–2009, https://doi.org/10.1175/1520-0442(1999)0121990:TENOSD>2.0.CO;2, 1999.
- Cai, W., and Cowan, T.: Trends in Southern Hemisphere circulation in IPCC AR4 models over 1950–99: Ozone depletion versus greenhouse forcing, J. Clim., 20, 681–693, https://doi.org/10.1175/JCLI4035.1, 2007.
- Chen, Z., Gan, B., Wu, L., and Jia, F.: Pacific–North American teleconnection and North Pacific Oscillation: Historical simulation and future projection in CMIP5 models, Clim. Dyn., 50, 4379–4403, https://doi.org/10.1007/s00382-017-3881-9, 2018.
 - Coburn, J., and Pryor, S. C.: Differential credibility of climate modes in CMIP6, J. Clim., 34, 8145–8164, https://doi.org/10.1175/JCLI-D-21-0359.s1, 2021.
 - Deser, C., Alexander, M. A., Xie, S. P., and Phillips, A. S.: Sea surface temperature variability: Patterns and mechanisms, Annu. Rev. Mar. Sci., 2, 115–143, https://doi.org/10.1146/annurev-marine-120408-151453, 2010.
 - Deser, C., Knutti, R., Solomon, S., and Phillips, A. S.: Communication of the role of natural variability in future North American climate, Nat. Clim. Change, 2, 775–779, https://doi.org/10.1038/nclimate1562, 2012.
- Deser, C., and Phillips, A. S.: Defining the internal component of Atlantic Multidecadal Variability in a changing climate, Geophys. Res. Lett., 48, 1–10, https://doi.org/10.1029/2021GL095023, 2021.





- Dong, L., and McPhaden, M. J.: The role of external forcing and internal variability in regulating global mean surface temperatures on decadal timescales, Environ. Res. Lett., 12, 1–10, https://doi.org/10.1088/1748-9326/AA5DD8, 2017.
- Fasullo, J. T., Phillips, A., and Deser, C.: Evaluation of leading modes of climate variability in the CMIP archives, J. Clim., 33, 5527–5545, https://doi.org/10.1175/JCLI-D-19-1024.1, 2020.
 - Flato, G., et al.: Evaluation of climate models, in: Climate Change 2013: The Physical Science Basis, T. F. Stocker et al. (eds.), Cambridge University Press, 741–866, 2013.
- Folland, C. K., Renwick, J. A., Salinger, M. J., and Mullan, A. B.: Relative influences of the Interdecadal Pacific Oscillation and ENSO on the South Pacific Convergence Zone, Geophys. Res. Lett., 29, 21–1, https://doi.org/10.1029/2001GL014201, 2002.
 - Gong, D., and Wang, S.: Definition of Antarctic Oscillation index, Geophys. Res. Lett., 26, 459–462, https://doi.org/10.1029/1999GL900003, 1999.
- Hannachi, A., Jolliffe, I. T., and Stephenson, D. B.: Empirical orthogonal functions and related techniques in atmospheric science: A review, Int. J. Climatol., 27, 1119–1152, https://doi.org/10.1002/joc.1499, 2007.
 - Henley, B. J., Gergis, J., Karoly, D. J., Power, S., Kennedy, J., and Folland, C. K.: A Tripole Index for the Interdecadal Pacific Oscillation, Clim. Dyn., 45, 3077–3090, https://doi.org/10.1007/s00382-015-2525-1, 2015.
- Henley, B. J., Meehl, G., Power, S. B., Folland, C. K., King, A. D., Brown, J. N., et al.: Spatial and temporal agreement in climate model simulations of the Interdecadal Pacific Oscillation, Environ. Res. Lett., 12, 1–10, https://doi.org/10.1088/1748-9326/AA5CC8, 2017.
 - Hersbach, H., Bell, B., Berrisford, P., Hirahara, S., Horányi, A., Muñoz-Sabater, J., et al.: The ERA5 global reanalysis, Q. J. Roy. Meteor. Soc., 146, 1999–2049, https://doi.org/10.1002/qj.3803, 2020.
 - Hobbs, W., Palmer, M. D., and Monselesan, D.: An energy conservation analysis of ocean drift in the CMIP5 global coupled models, J. Clim., 29, 1639–1653, https://doi.org/10.1175/JCLI-D-15-0477.1, 2016.
- Huang, B., Thorne, P. W., et al.: Extended Reconstructed Sea Surface Temperature version 5
 (ERSSTv5), Upgrades, validations, and intercomparisons, J. Clim., 30, 8179–8205, https://doi.org/10.1175/JCLI-D-16-0836.1, 2017.
 - Hurrell, J. W., and Deser, C.: North Atlantic climate variability: The role of the North Atlantic Oscillation, J. Mar. Syst., 78, 28–41, https://doi.org/10.1016/J.JMARSYS.2008.11.026, 2009.
- Hurrell, J. W., Kushnir, Y., Ottersen, G., and Visbeck, M.: An overview of the North Atlantic Oscillation, Geophys. Monogr. Ser., 134, 1–35, https://doi.org/10.1029/134GM01, 2003.
 - IPCC: Climate Change 2014: Synthesis Report, Geneva, Switzerland, 151 pp., 2014.
 - IPCC: Annex IV: Modes of Variability, in: Climate Change 2021: The Physical Science Basis, Masson-Delmotte, V., et al. (eds.), Cambridge University Press, Cambridge, United Kingdom and New York, NY, USA, 2153–2192, https://doi.org/10.1017/9781009157896.018, 2021.





- Izzaddin, A., Langousis, A., Totaro, V., Yaseen, M., and Iacobellis, V.: A new diagram for performance evaluation of complex models, Stoch. Environ. Res. Risk Assess., 38, 2261–2281, https://doi.org/10.1007/s00477-024-02678-3, 2024.
- Kavvada, A., Ruiz-Barradas, A., and Nigam, S.: AMO's structure and climate footprint in observations and IPCC AR5 climate simulations, Clim. Dyn., 41, 1345–1364, https://doi.org/10.1007/s00382-013-1712-1, 2013.
 - Kay, J. E., Deser, C., Phillips, A., Mai, A., Hannay, C., Strand, G., et al.: The Community Earth System Model (CESM) Large Ensemble Project: A Community Resource for Studying Climate Change in the Presence of Internal Climate Variability, Bull. Amer. Meteor. Soc., 96, 1333–1349, https://doi.org/10.1175/BAMS-D-13-00255.1, 2015.
- Krishnamurthy, V., and Kirtman, B. P.: Variability of the Indian Ocean: Relation to monsoon and ENSO, Q. J. Roy. Meteor. Soc., 129, 1623–1646, https://doi.org/10.1256/qj.01.166, 2003.
 - Lee, J., Sperber, K. R., Gleckler, P. J., Taylor, K. E., and Bonfils, C. J.: Benchmarking performance changes in the simulation of extratropical modes of variability across CMIP generations, J. Clim., 34, 6945–6969, https://doi.org/10.1175/JCLI-D-20-0832.1, 2021.
- 665 Marshall, G. J.: Trends in the Southern Annular Mode from observations and reanalyses, J. Clim., 16, 4134–4143, <a href="https://doi.org/10.1175/1520-0442(2003)016<4134:TITSAM>2.0.CO">https://doi.org/10.1175/1520-0442(2003)016<4134:TITSAM>2.0.CO; 2, 2003.
 - McKenna, S., Santoso, A., Gupta, A. S., et al.: Indian Ocean Dipole in CMIP5 and CMIP6: characteristics, biases, and links to ENSO, Sci. Rep., 10, 1–10, https://doi.org/10.1038/s41598-020-68268-9, 2020.
 - Meehl, G. A., and Arblaster, J. M.: Relating the strength of the tropospheric biennial oscillation (TBO) to the phase of the Interdecadal Pacific Oscillation (IPO), Geophys. Res. Lett., 39, 1–10, https://doi.org/10.1029/2012gl053386, 2012.
- Miller, R. L., Schmidt, G. A., and Shindell, D. T.: Forced annular variations in the 20th century Intergovernmental Panel on Climate Change fourth assessment report models, J. Geophys. Res., 111, 1–10, https://doi.org/10.1029/2005JD006323, 2006.
 - Mohapatra, S., and Gnanaseelan, C.: A new mode of decadal variability in the Tropical Indian Ocean subsurface temperature and its association with shallow meridional overturning circulation, Glob. Planet. Change, 207, 1–10, https://doi.org/10.1016/j.gloplacha.2021.103656, 2021.
 - Mohapatra, S., Gnanaseelan, C., Fousiya, T. S., and Dandapat, S.: What drives the decadal variability in sea surface salinity and stratification over the tropical Indian Ocean?, Theor. Appl. Climatol., 152, 1–10, https://doi.org/10.1007/s00704-023-04429-w, 2023.
- Mohapatra, S., Sen Gupta, A., Bindoff, N. L., and Lyu, Y.: Climate Mode Datasets and Generating Codes from CMIP6 Pre-Industrial Control Simulations and Observations, Zenodo, 1–10, https://doi.org/10.5281/zenodo.17337105, 2025.
 - Park, J. Y., Schloesser, F., Timmermann, A., Choudhury, D., Lee, J. Y., and Nellikkattil, A. B.: Future sea-level projections with a coupled atmosphere-ocean-ice-sheet model, Nat. Commun., 14, 1–10, https://doi.org/10.1038/s41467-023-36051-9, 2023.





- Planton, Y. Y., et al.: Evaluating climate models with the CLIVAR 2020 ENSO metrics package, Bull. Amer. Meteor. Soc., 102, E193–E217, https://doi.org/10.1175/BAMS-D-19-0337.1, 2021.
- Power, S., Casey, T., Folland, C., Colman, A., and Mehta, V.: Inter-decadal modulation of the impact of ENSO on Australia, Clim. Dyn., 15, 319–324, https://doi.org/10.1007/s003820050284, 1999.
 - Rhein, M., Rintoul, S. R., Aoki, S., Campos, E., Chambers, D., Feely, R. A., et al.: Observations: Ocean, in: Climate Change 2013: The Physical Science Basis, Cambridge University Press, Cambridge, United Kingdom and New York, NY, USA, 1–100, 2013.
- Saji, N. H., Goswami, B. N., Vinayachandran, P. N., and Yamagata, T.: A dipole mode in the tropical Indian Ocean, Nature, 401, 360–363, https://doi.org/10.1038/43854, 1999.
 - Sayantani, O., and Gnanaseelan, C.: Tropical Indian Ocean subsurface temperature variability and the forcing mechanisms, Clim. Dyn., 44, 2447–2462, https://doi.org/10.1007/s00382-014-2379-y, 2015.
- Schulz, M., and Mudelsee, M.: REDFIT: estimating red-noise spectra directly from unevenly spaced paleoclimatic time series, Comput. Geosci., 28, 421–426, https://doi.org/10.1016/S0098-3004(01)00044-9, 2002.
 - Sen Gupta, A., Jourdain, N. C., Brown, J. N., and Monselesan, D.: Climate drift in the CMIP5 models, J. Clim., 26, 1–10, https://doi.org/10.1175/JCLI-D-12-00521.s1, 2013.
- Taschetto, A. S., Rodrigues, R. R., Meehl, G. A., McGregor, S., and England, M. H.: How sensitive are the Pacific-tropical North Atlantic teleconnections to the position and intensity of El Niño-related warming?, Clim. Dyn., 46, 1841–1860, https://doi.org/10.1007/s00382-015-2679-x, 2015.
 - Taylor, K. E.: Summarizing multiple aspects of model performance in a single diagram, J. Geophys. Res., 106, 7183–7192, https://doi.org/10.1029/2000JD900719, 2001.
- Wang, Y., Li, S., and Lu, D.: Seasonal response of Asian monsoonal climate to the Atlantic Multidecadal Oscillation, J. Geophys. Res. Atmos., 114, 1–10, https://doi.org/10.1029/2008JD010929, 2009.
 - Webster, P. J., Moore, A. M., Loschnigg, J. P., and Leben, R. R.: Coupled ocean–atmosphere dynamics in the Indian Ocean during 1997–98, Nature, 401, 356–360, https://doi.org/10.1038/43848, 1999.
 - Wilks, D. S.: Statistical methods in the atmospheric sciences, 3rd edn., Elsevier/Academic Press, Amsterdam, Boston, 1–650, 2011.
- Xu, K., Tam, C.-Y., Zhu, C., and Liu, B.: CMIP5 projections of two types of El Niño and their related tropical precipitation in the twenty-first century, J. Clim., 30, 1–10, https://doi.org/10.1175/JCLI-D-16-0413.s1, 2017.
 - Zuo, H., Balmaseda, M. A., Tietsche, S., Mogensen, K., and Mayer, M.: The ECMWF operational ensemble reanalysis-analysis system for ocean and sea-ice: A description of the

https://doi.org/10.5194/essd-2025-618 Preprint. Discussion started: 11 November 2025 © Author(s) 2025. CC BY 4.0 License.





system and assessment, Ocean Sci. Discuss., 15, 779–808, https://doi.org/10.5194/os-2018-154, 2018.